Polymer 298 (2024) 126869

Contents lists available at ScienceDirect

Polymer

journal homepage: www.elsevier.com/locate/polymer

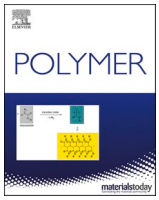

In situ polymerised polyaniline films over multi-walled carbon nanotubes coatings for enhanced photoelectrochemical performance

Alessandra A. Correa [a,b,1], Moisés A. de Araújo [c,†,1], Lucia H. Mascaro [c], Luiz H.C. Mattoso [a,b], José M. Marconcini [a,b,*]

[a] Departamento de Engenharia de Materiais, Universidade Federal de São Carlos, Rodovia Washington Luiz, km 235, postcode: 13565-905, Brazil
[b] Embrapa Instrumentação, Rua XV de Novembro, 1452, postcode: 13560-970, São Carlos, São Paulo, Brazil
[c] Departamento de Química, Universidade Federal de São Carlos, Rodovia Washington Luiz, km 235, postcode: 13565-905, São Carlos, São Paulo, Brazil

ARTICLE INFO

Keywords:
π-conjugated polymers
Carbon
Solar-driven water splitting
Hydrogen

ABSTRACT

Polyaniline (PANI), which is a π-conjugated polymer, has stood out as a promising candidate for dihydrogen generation in photoelectrochemical (PEC) cells owing to its suitable optoelectronic properties and excellent stability. Nevertheless, the PEC performance of this material is still far from adequate for technological applications. Herein, we have focused on improving the PEC performance of PANI films by combining this polymer with multi-walled carbon nanotubes (MWCNTs) layers. Specifically, we have assessed the PEC activity of the in situ polymerised PANI films onto FTO substrates coated with different amounts of MWCTNs for the hydrogen evolution reaction (HER). The FTO/MWCNTs/PANI films with the optimum deposited amount of MWCNTs (i.e., 30 μL) featured a 2.4-fold increase of the cathodic photocurrent density response for the HER compared to that of FTO/PANI film. Moreover, the FTO/(30 μL)-MWCNTs/PANI films exhibited good PEC stability, as observed by the relatively low cathodic photocurrent density decay of up to 7% during 3720 s of stability test. Based on joint analyses of physical and PEC characterisation, the improved PEC performance for the FTO/(30 μL)-MWCNTs/PANI films were assigned to the combined contribution of the following factors: (i) enhancement of light absorption; (ii) possible improvement of excitons dissociation; (iii) minimisation of the electron-hole recombination process; and (iv) facilitation of electrons transfer at the PANI|electrolyte interface for the HER. The enhancement of PEC performance achieved in this work for the fully organic photocathode composed of MWCNTs/PANI paves the way to invest in additional modifications seeking to further improve the dissociation of excitons and the interfacial transfer of charge carriers for the light-driven HER.

1. Introduction

Harvesting solar energy in photoelectrochemical (PEC) cells has been highly regarded as a sustainable approach to obtaining dihydrogen (H_2) via solar-driven water splitting. Being a clean energy carrier, H_2 can potentially become one of the mainstream energy sources in the future, due to its superior energy yield compared to conventional hydrocarbon fuels [1]. In addition to PEC cells, it has also been reported alternative approaches, such as electrolysers and hybrid devices (i.e., electrolysers combined with photovoltaic cells), to obtain H_2 via water splitting [2]. Among these systems, PEC cells have the advantage of possessing a simpler system configuration with a lower fabrication cost compared to the electrolysers coupled to photovoltaic cells [2].

Considering the PEC cells system, H_2 can be generated from water splitting and this process takes place on the photocathode (i.e., a p-type semiconductor) via hydrogen evolution reaction (HER) under illumination. For a high performance of this reaction, it is expected, among other requirements, that the photocathode features highly efficient photon absorption over a wide range of the solar spectrum and provides a fast transfer of the photogenerated carriers at the photocathode|

* Corresponding author. Departamento de Engenharia de Materiais, Universidade Federal de São Carlos, Rodovia Washington Luiz, km 235, postcode: 13565-905, Brazil.
E-mail address: jose.marconcini@embrapa.br (J.M. Marconcini).
† Present address: Instituto de Química de São Carlos, Universidade de São Paulo, Avenida Trabalhador Sancarlense, 400, postcode: 13566-590, São Carlos, São Paulo, Brazil.
[1] These authors contributed equally to the present work.

https://doi.org/10.1016/j.polymer.2024.126869
Received 28 November 2023; Received in revised form 28 February 2024; Accepted 1 March 2024
Available online 2 March 2024

electrolyte interface [3]. To meet these requirements, a variety of inorganic semiconductor materials has been under consideration for H_2 generation in PEC cells. Some of the promising photocathode candidates include, e.g., sulphides- and selenides-based semiconductors [4–8]. Besides the inorganic semiconductors, carbon-based materials, such as π-conjugated polymers, have also recently driven notorious interest due to their electronic structure that can be more easily tuned to enhance solar energy harvesting compared with inorganic semiconductors [9]. As Additional advantages of π-conjugated polymers compared to inorganic semiconductors, polymers are comprised of earth-abundant elements, namely, C, N, O and H, and the fabrication of polymer-based photoelectrodes is often less complex and involves low-cost methodologies at ambient conditions [9], which are desirable for large-scale applications. For PEC water splitting application, some of the π-conjugated polymers feature the desirable following characteristics: (i) high absorption coefficient in the visible region of the solar spectrum; (ii) high charge carrier mobility; and (iii) suitable energy levels of the lowest unoccupied molecular orbital (LUMO) and highest occupied molecular orbital (HOMO) that favours the occurrence of HER and oxygen evolution reaction (OER), respectively, under illumination [3,10].

Among the π-conjugated polymers, polyaniline (PANI) has drawn considerable attention for H_2 generation via PEC water splitting due to its adequate potential of the LUMO that enables the transfer of the photogenerated electrons for the occurrence of the light-driven HER. Other unique properties of PANI are the high absorbance coefficient encompassing a wide spectral range (i.e., from visible to infrared region), non-toxic, and p-type conductivity [11], meaning that it can be used as a photocathode in PEC cells. It is also important to mention the chemical structure of PANI, whose general formula is $[(-bz-NH-bz-NH-)_x(-bz-N=qn=N-)_{1-x}]_n$, where bz is the benzenoid ring and qn is the quinoid ring. This molecular formula changes with its oxidation state and three oxidation states can be found, namely leucoemeraldine base (fully reduced) for $x = 1$, emeraldine base (half reduced and half oxidised) for $x = 0.5$, and pernigraniline base (fully oxidised) for $x = 0$ [12]. The emeraldine base form of PANI can also be converted into the emeraldine salt form of PANI via protonation with inorganic or organic acids. Among these different oxidation states of PANI, the emeraldine salt form stands advantageous for PEC cell application due to its high electron transfer performance and narrow optical bandgap [11].

Despite having suitable optoelectronic properties for PEC water splitting, π-conjugated polymers in general feature poor dissociation of the photogenerated excitons (i.e., bound electron-hole pairs) [13,14], and such a dissociation process is a fundamental step for the generation of free charge carriers (i.e., electrons and holes) to trigger the HER or OER at the polymer|electrolyte interface. Another limiting factor is the fast charge carriers' recombination either at the surface or in the bulk of π-conjugated polymers [14], which greatly compromises their PEC performance. One way to improve excitons dissociation and minimise recombination effect is via combining π-conjugated polymer, e.g., graphitic carbon nitride (g-C_3N_4), with carbon nanotubes (CNTs) to form a composite or a heterojunction [15]. The employment of CNTs stands advantageously due to their unique properties, such as high specific surface area, hollow structures, and good conductivity [16], which can be beneficial in PEC cells. CNTs also stand advantageous compared to other carbon-based materials such as graphene, which is CNTs unrolled structure into graphene layers, because CNTs have larger surface area than graphene [17], and this can contribute to improving PEC water splitting. It is also important to mention that it has been demonstrated that the combination of multi-walled carbon nanotubes (MWCNTs), which is a variant of CNTs, with, for example, g-C_3N_4, can improve photocatalytic H_2 generation, and that was assigned to the effective charge transfer process and increase of active sites available [18]. In another study, Chen et al. [19] showed that the MWCNTs/g-C_3N_4 composite favoured an increase in the charge carriers' lifetime compared to that of pure g-C_3N_4, which was beneficial for the enhancement of photocatalytic H_2 generation.

Regarding the studies about fully organic photoelectrodes comprised of CNTs/PANI films for light-driven HER, to the best of our knowledge, this kind of system has not been endeavoured yet. Studies have been focused on addressing the CNTs/PANI composite films in a wide variety of applications, including, e.g., supercapacitors [20–22], thermoelectric materials [23], and sensors [24]. It has been recently shown that improvement of photocatalytic H_2 generation can be achieved via the employment of composites made up of PANI and inorganic materials, such as Ti/Ti–W@PANI [25], Cu/BN@PANI [26], and TiO_2-PANI-Au [27]. Another study has also demonstrated improvement of PEC performance for H_2 generation on the ITO/PANI/P3HT:PCBM/TiO_x/Pt films, in which PANI films were obtained by electrochemical polymerisation [28].

In light of what has been presented, the main motivation of the present work is to investigate the PEC performance of an organic photoelectrode comprised of PANI films having an MWCNTs underlayer. The MWCNTs layers and the PANI films were obtained by drop casting and in situ chemical oxidative polymerisation of aniline, respectively, which are both simple (not requiring sophisticated systems), economical, and scalable methodologies for films preparation. Herein, we have specifically assessed the PEC HER performance of the FTO/MWCNTs/PANI films featuring MWCNTs layers deposited with different amounts. As will be shown, the presence of the MWCNTs underlayer led to an improvement of PEC response for HER and good stability of the FTO/MWCNTs/PANI films. Based on the physical and PEC characterisation analyses of the films, the improvement of PEC performance was assigned to the combined effect of different factors, namely enhanced light absorption, possible improvement of excitons dissociation and minimised recombination process, and facilitation of electrons transfer at the PANI|electrolyte interface for the HER.

2. Methods and materials

2.1. Reagents

The aniline ($C_6H_5NH_2$, Sigma-Aldrich, ≥ 99.5%) was vacuum distilled under dinitrogen (N_2) prior to use, and all the other reagents were used as received. The main chemical reagents employed in this work were hydrochloric acid (HCl, Synth, 37%), ammonium peroxydisulphate (APS) ($(NH_4)_2S_2O_8$, Neon, ≥ 98.0%), MWCNTs (Shenzhen Nanotech Port, > 97%, length and diameter of 5–15 μm and 20–40 nm, respectively), and sodium sulphate (Na_2SO_4, Synth, 99.0%). All the aqueous solutions were prepared with ultra-purified water (resistivity of 18.2 MΩ cm) from a Milli-Q® system.

2.2. Preparation of FTO/MWCNTs coatings

The MWCNTs were first pre-treated using a solution of concentrated sulphuric and nitric acids in the volumetric proportion of 3:1 v/v. The mixture was stirred for 12 h at room temperature with subsequent filtering and washing of the MWCNTs. At last, the MWCNTs were dried in an oven for 12 h at 70 °C. Once the MWCNTs were pre-treated, a suspension of it was prepared by adding 1.0 mg of MWCNTs into 1.0 mL of dimethylformamide (DMF) and then stirred in an ultrasonic bath for 30 min. The pre-treatment with the acidic mixture, also known as oxidative treatment, aimed to chemically functionalise the MWCNTs with functional groups of carboxyl, hydroxyl and/or ketone [29], which provides better dispersibility of the MWCNTs in DMF [30]. Additionally, the chemical functionalisation of MWCNTs aimed to enhance the interaction between MWCNTs and PANI [29].

The MWCNTs coatings were obtained by placing an aliquot of 10, 30, or 50 μL of the MWCNTs suspension on FTO substrates (Sigma-Aldrich, surface resistivity of ≈ 7 Ω/sq), which was previously cleaned as reported somewhere else [31]. The FTO substrates containing the different MWCNTs aliquots were then left to dry out at room temperature to form

the MWCNTs coatings.

2.3. Preparation of FTO/MWCNTs/PANI films

The in situ preparation of the PANI films consisted of placing the MWCNTs-coated FTO substrates in an upright position into a solution comprised of 10 mL of 0.2 mol L^{-1} HCl and 91 μL of 0.1 mol L^{-1} distilled aniline. At this stage, the temperature of the system was maintained at 0–5 °C (an ice bath was used to control the temperature) and then 10 mL of 0.1 mol L^{-1} APS was added slowly into this solution under stirring. Once elapsed 1 h of the polymerisation reaction onto the substrate, the films were dipped in 0.1 mol L^{-1} HCl and then thoroughly rinsed with ultra-purified water. For the sake of comparison, PANI films were also prepared on bare FTO substrate by following this procedure.

2.4. PEC measurements of FTO/MWCNTs/PANI films

The PEC measurements aimed to evaluate the photoelectroactivity of the FTO/MWCNTs/PANI films for H_2 generation via light-driven water splitting. It was employed as the analysis parameter, the cathodic photocurrent density signal generated by the films since it is directly proportional to the amount of H_2 generated. This parameter was obtained via chronoamperometry measurements at −0.5 V vs. Ag/AgCl/$Cl^-_{(sat.\ KCl)}$ and under chopped or constant illumination. The illumination source was a UV LED (ThorsLabs M365LP1) with a wavelength of 365 nm, and an irradiance of ca. 100 mW cm^{-2}.

To further understand the PEC performance of the films, electrochemical impedance spectroscopy (EIS) experiments were carried out for the films polarised at −0.5 V vs. Ag/AgCl/$Cl^-_{(sat.\ KCl)}$ and under constant UV illumination. The impedance spectra were recorded at a frequency range from 100 kHz to 0.2 Hz and an amplitude of 10 mV_{RMS}. The ZView (version 3.1c) software was employed to model the impedance spectra into an equivalent electric circuit.

The chronoamperometries and impedance spectra were recorded in a potentiostat/galvanostat (Autolab PGSTAT302 N) controlled by the Nova software (version 1.10.4) and using a three-electrode cell configuration containing a quartz window. The working electrode was the MWCNTs/PANI films deposited onto the FTO substrate (geometric area of ≈ 1.0 cm^2). The counter and reference electrodes were a platinum plate (geometric area of ≈ 1.2 cm^2) and an Ag/AgCl/$Cl^-_{(sat.\ KCl)}$ electrode, respectively. All the potential values presented in this work are with respect to this reference electrode (unless specified by another reference electrode). The PEC experiments were performed in an electrolyte comprised of 0.5 mol L^{-1} Na_2SO_4 at pH 2.0 (pH adjusted with diluted H_2SO_4) saturated with N_2.

2.5. Physical characterisation of FTO/MWCNTs/PANI films

The morphological characterisation of the films was performed using a high-resolution field emission scanning electron microscope (FE-SEM, Zeiss Supra™ 35). This analysis was also carried out, for some of the films, on an FEG (Jeol JSM-6701F). The absorbance and reflectance spectra of the films were recorded in an ultraviolet–visible–near-infrared (UV–vis–NIR) spectrophotometer (Varian Cary 5).

A Raman spectrometer (Bruker Senterra) was employed for the structural characterisation of the films. The excitation source was a laser beam having a wavelength of 532 nm and a power of 5 mW. Each spectrum was obtained with a resolution of 3–5 cm^{-1} and an integration time of 5 s. Additional structural characterisation of the films was performed using a Fourier transform infrared (FTIR) spectrometer (Thermo Nicolet Nexus 670) containing an attenuated total reflectance (ATR) accessory.

3. Results and discussion

Before delving into the evaluation of physical and PEC characterisation of the FTO/MWCNTs/PANI films, it is important to mention that the in situ polymerised PANI films obtained on FTO substrates featured a green colour (Fig. 1a). As widely documented in the literature [11,24,32], PANI films having this colour imply the formation of the emeraldine salt form of PANI, or more specifically in this work, PANI in the form of emeraldine hydrochloride which could assume either polaronic or bipolaronic structure [33] (see Fig. 1b). For the PANI films in situ grown on MWCNTs-coated FTO substrates, these films were dark green (Fig. 1a), which is also characteristic of the emeraldine salt form of PANI. In terms of the polymerisation mechanism of PANI films on a solid surface via the chemical oxidation of aniline, it is believed that it may involve the following three main steps: (i) adsorption of aniline oligomers, which is formed by the oxidation of aniline in an acidic aqueous medium having, e.g., APS; (ii) nucleation, i.e., the adsorbed oligomers react to form the first PANI chain, also known as a nucleus of the future film; and (iii) film growth, which is characterised by the formation of other PANI chains due to the auto-accelerated polymerisation of aniline [34]. This process means that new oligomers are formed and adsorbed close to the nucleus and subsequently react to form new PANI chains. The PANI film formation is a result of the proliferation of the PANI chains along the surface, and the PANI chains are usually oriented perpendicularly to the surface of the substrate [34]. Regarding specifically the in situ grown mechanism of PANI films on FTO substrates, to the best of our knowledge, this mechanism has not been studied yet. However, based on reported studies for PANI films grown on glass [35], which share similarities with the mechanism described previously, we believe that the mechanism for the formation of PANI films over FTO-coated glass substrates may occur probably in a similar way. For the mechanism of the in situ formation of PANI films over the MWCNTs layer, to the best of our knowledge, it has not been investigated yet. Studies have shown that the formation of the MWCNTs/PANI system is due to the electrostatic interaction and π-π stacking between the aromatic structure and the graphite surface [36]. It is important to mention that a detailed analysis of the in situ growth mechanism of PANI films on FTO and FTO/MWCNTs substrates is beyond the scope of this work, as our primary aim was to obtain the FTO/MWCNTs/PANI films and apply them for H_2 generation via solar-driven water splitting.

Prior to present the results of the PEC water splitting application, we initially fully characterised the in situ obtained PANI films on bare and coated FTO substrates with different amounts of MWCNTs (i.e., 10, 30, and 50 μL). The physical characterisation of the films is presented as follows.

3.1. Physical characterisation of the films

Regarding the morphological analysis of the FTO/MWCNTs/PANI films, we have initially assessed the morphology of the MWCNTs films with different amounts deposited on FTO substrates. As shown by the scanning electron microscopy (SEM) micrographs in Fig. 2, the (10 μL)-, (30 μL)-, and (50 μL)-MWCNTs films featured fibre-like structures, and the maximum width of these fibres ranged from 25 to 45 nm (see the histograms in Fig. 2). It is important to mention that the scale bar length of the SEM micrograph for the FTO/(30 μL)-MWCNTs film is different compared to the other samples because two different brands of scanning electronic microscopes were employed. Nevertheless, this did not compromise the comparison of SEM micrographs of the different samples, since, as expected, all the films featured similar values of MWCNTs maximum width.

Concerning the SEM analyses of the PANI films (Fig. 3), the PANI films deposited over FTO substrates featured, in terms of morphology, closely packed structures of granular or round-shaped agglomerations as well as clusters formation having irregular size and shape. Different from the morphology observed for PANI films deposited on bare FTO substrates, the PANI films grown on MWCNTs-coated FTO substrates featured fibre-like structures, and such structures were observed for all the amounts of MWCNTs employed to coat the FTO substrates. The

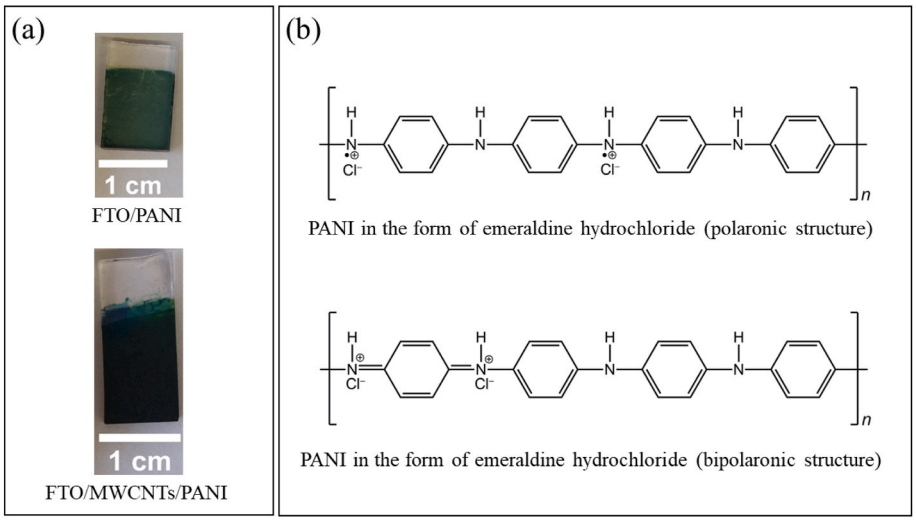

Fig. 1. (a) Photographs of FTO/PANI and FTO/MWCNTs/PANI films, and (b) polaronic and bipolaronic chemical structures of PANI in the form of emeraldine hydrochloride.

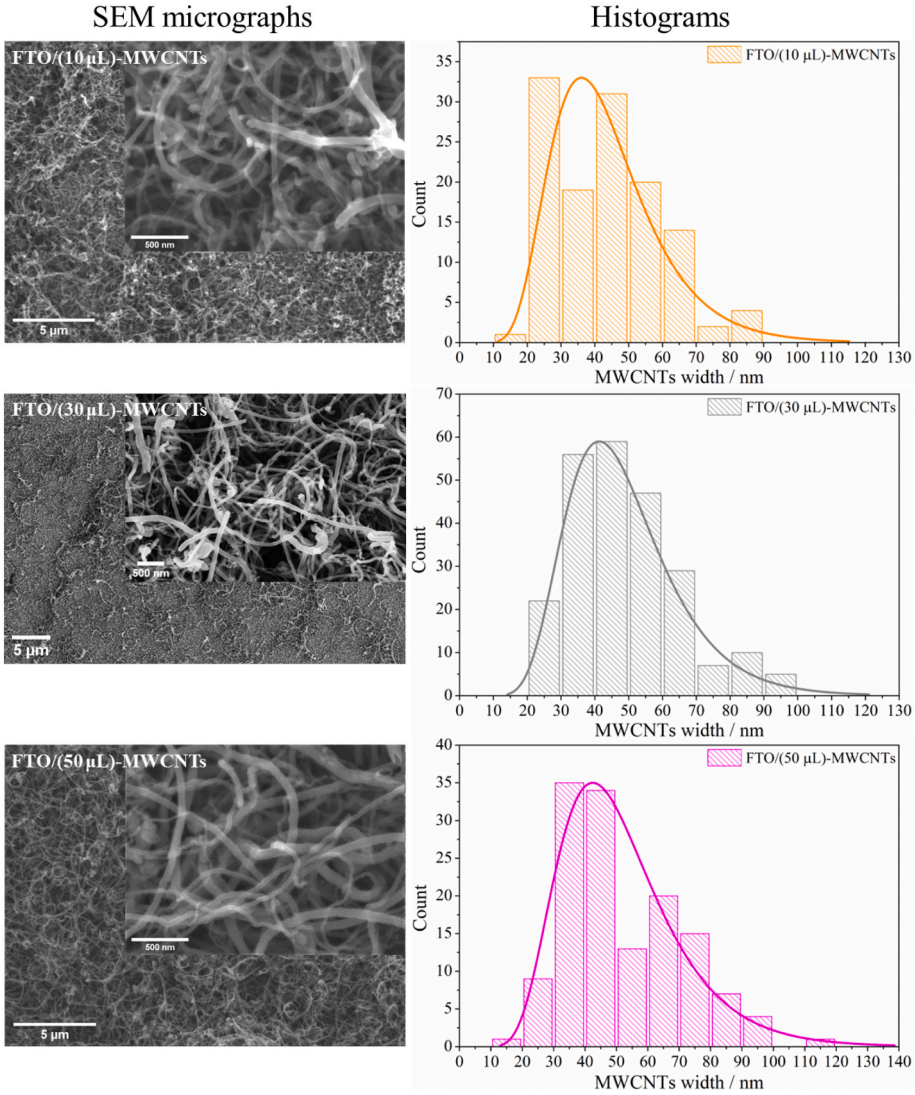

Fig. 2. SEM micrographs with magnifications of 5000 and 50,000 times (inset figure) and histograms of MWCNTs width distribution for MWCNTs films with different amounts deposited on FTO substrates.

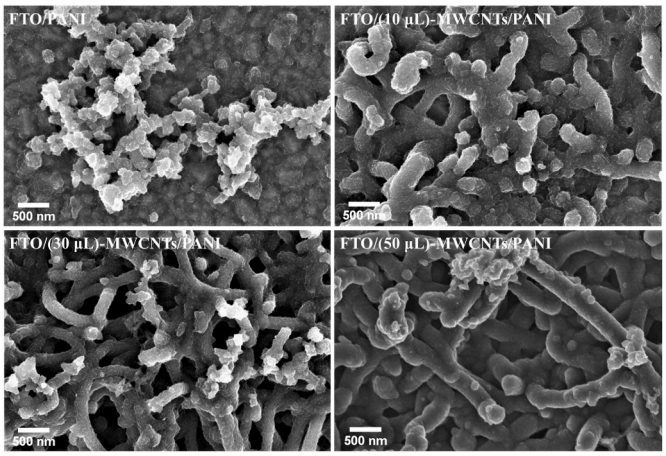

Fig. 3. SEM micrographs with a magnification of 50,000 times for PANI films grown on bare and coated FTO substrates with different amounts of MWCNTs.

maximum width of the fibres ranged approximately between 170 nm and 310 nm for the PANI films obtained on FTO coated with different amounts of MWCNTs (Figure S1 in the support information). Another interesting feature of the FTO/MWCNTs/PANI system is that the PANI's fibres appear to be arranged in a way that resembles pores and this was not observed for the FTO/PANI system. It is also noted the PANI films deposited on FTO substrates coated with different amounts of MWCNTs seem to have a rougher surface compared to the PANI films grown on FTO substrates (see Figure S2), and this may be due to the presence of wriggly PANI chains spread out on the FTO/MWCNTs/PANI films surface.

In addition to the morphology characterisation, we have also obtained the UV–vis–NIR spectra (see Fig. 4) to optically characterise the film that provided the optimum PEC performance (as will be shown later), namely FTO/(30 μL)-MWCNTs/PANI film. For the sake of comparison, we have also recorded the UV–vis–NIR spectra for the FTO/PANI and FTO/(30 μL)-MWCNTs films. As shown in Fig. 4a, the absorbance spectrum of the FTO/PANI film featured a broad band centred at ca. 710 nm and a shoulder band at ca. 430 nm. The former one is assigned to the π → polaron transition [37], whilst the latter one is attributed to the polaron → π* transition [37], which suggests the occurrence of the PANI emeraldine salt [38,39]. It was also noted an absorption region in the range of 350 and ca. 400 nm and that is ascribed to the π → π* transition in the aromatic rings [38,40]. Regarding the absorbance spectrum of the FTO/(30 μL)-MWCNTs/PANI film, it was not noted additional bands, nevertheless, a slight blue shift was observed for the band assigned to the π → polaron transition, which could have been due to the increase of interaction energy between the PANI film and the MWCNTs layer [41,42]. Concerning the nature of this interaction, we believe it is associated with the π-π interaction between probably the quinoid rings of the PANI and the π-conjugated structure of the MWCNTs [43,44]. Still regarding the absorbance spectrum of the FTO/(30 μL)-MWCNTs/PANI film, it is critical to note that the FTO/(30 μL)-MWCNTs/PANI film featured an absorbance increase in a wide range of the UV–vis–NIR region (i.e., from 350 to 1300 nm) compared to that of FTO/PANI film. This improvement is possibly linked to the porous structure of the FTO/(30 μL)-MWCNTs/PANI film (Fig. 3), which may have provided more chances for light absorption via the multiple reflections and scattering of the incident light within the porous structure of this film [45]. Concerning the absorbance spectrum of the FTO/(30 μL)-MWCNTs film, we have not observed absorbance bands in the region of 350–1800 nm, which means that the MWCNTs did not significantly contribute to the absorption of light and such a phenomenon is exclusively governed by the PANI. To further evaluate the light absorption effect, transmittance (the inset of Fig. 4a) and reflectance (see Fig. 4b) spectra of the films have also been recorded. One notices that both transmittance (from 350 to 1317 nm) and reflectance (from 350 to 797 nm) decreased in values for the FTO/(30 μL)-MWCNTs/PANI film compared to that of FTO/PANI film, which further verifies that the FTO/(30 μL)-MWCNTs/PANI film favours light absorption.

Additional characterisation of the FTO/(30 μL)-MWCNTs/PANI film as well as the FTO/PANI and FTO/(30 μL)-MWCNTs films has been performed via ATR-FTIR spectroscopy. For comparison purposes, we have also recorded the ATR-FTIR spectrum of the FTO substrate. As displayed in Fig. 5, the bands displayed within the wavenumber region

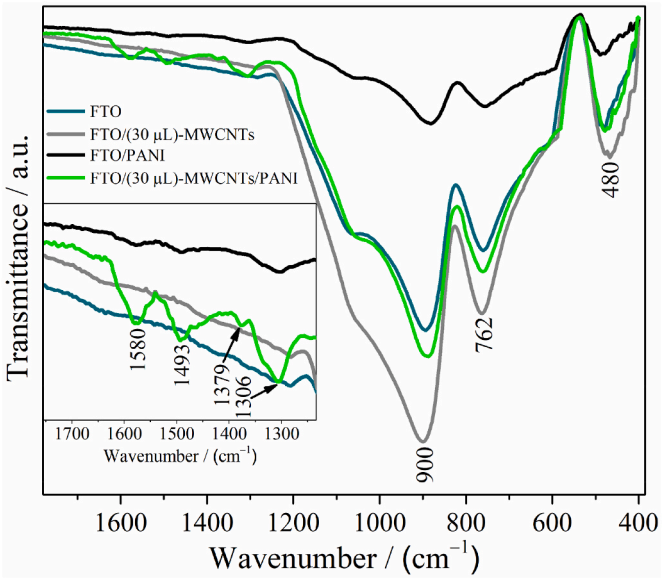

Fig. 5. ATR-FTIR spectra of FTO/(30 μL)-MWCNTs, FTO/PANI and FTO/(30 μL)-MWCNTs/PANI films, and FTO substrate.

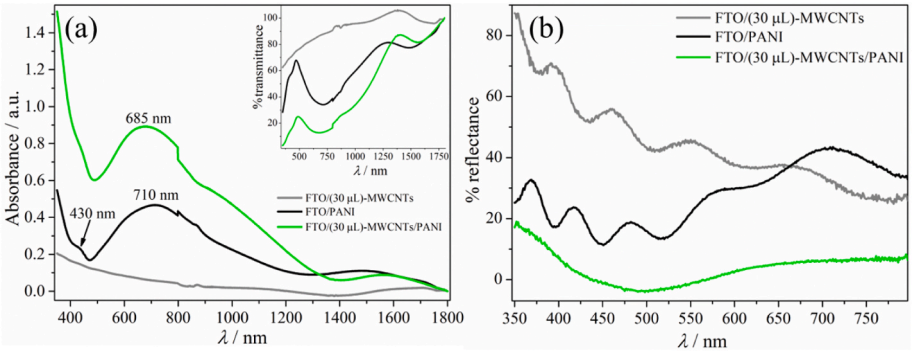

Fig. 4. (a) Absorbance, transmittance (inset figure), and (b) reflectance spectra of FTO/(30 μL)-MWCNTs, FTO/PANI, and FTO/(30 μL)-MWCNTs/PANI films.

of 400 and 1250 cm^{-1} are characteristics of the SnO_2 from the FTO. For such a region, the bands centred at ca. 480 and 762 cm^{-1} are assigned to the Sn–O and Sn–O–Sn vibrations of SnO_2 [46], and the band centred at ca. 900 cm^{-1} is attributed to the Sn–OH vibration mode [47]. PANI has also presented bands in the ATR-FTIR spectra, which have become more evident under the presence of the MWCNTs. Regarding the ATR-FTIR spectrum of the FTO/(30 μL)-MWCNTs/PANI film, the bands centred at ca. 1580 and 1493 cm^{-1} are ascribed to the C═C stretching of the quinoid and benzenoid rings, respectively, of PANI [48–50]. The presence of these bands confirms the formation of PANI in the emeraldine salt form of PANI [49,51,52], which is consistent with the observations of the absorbance spectra (Fig. 4a). It was also noted other bands centred at ca. 1379 and 1306 cm^{-1} attributed to the C–N stretching of the quinoid and benzenoid units, respectively, of PANI [50,53]. Concerning the ATR-FTIR spectrum of the FTO/(30 μL)-MWCNTs film, it has no observed bands for this material in the wavenumber range of 400 and 1780 cm^{-1}.

To complement the analyses of the ATR-FTIR spectra, we have also obtained the Raman spectra of the FTO/(30 μL)-MWCNTs, FTO/PANI, and FTO/(30 μL)-MWCNTs/PANI films. As shown in Fig. 6, the Raman spectrum of the FTO/(30 μL)-MWCNTs film featured two typical bands at 1350 (D mode) and 1580 cm^{-1} (G mode). The D band (disorder band) is assigned to the A_{1g} symmetrical stretching originating from the disordered carbon structure and defects of CNTs, and the G band (graphitic band) is attributed to the tangential phonon modes [54]. Regarding the Raman spectra of the FTO/PANI and FTO/(30 μL)-MWCNTs/PANI films, it was noted that these spectra featured a similar profile. Moreover, these spectra presented a band at ca. 1336 cm^{-1} which is assigned to the C–$N^{\bullet+}$ stretching of the bipolaron structure [39,55,56], thereby confirming the presence of emeraldine salt form of PANI as also observed by the absorbance (see Fig. 4a) and ATR-FTIR spectra (Fig. 5). It should be remarked that the emeraldine salt form of PANI can have a polaronic or bipolaronic structure (see Fig. 1b) [33], and these two structures can also coexist in the polymer [55]. Herein, we believe that the bipolaronic form is the major structure of the obtained PANI films since most of the bands of the Raman spectra of both FTO/PANI and FTO/(30 μL)-MWCNTs/PANI films were assigned to this structure. In terms of band assignment, the following bands of the spectra were attributed to the bipolaronic structure: 1487 (C–C stretching and C–H deformation), 1218 (C–N–C deformation), 1162 (C–H bending), 815 (C–H quinoid deformation), 775 (CNC and deformation), 546 (quinoid ring deformation), and 413 cm^{-1} (C–H wag) [55].

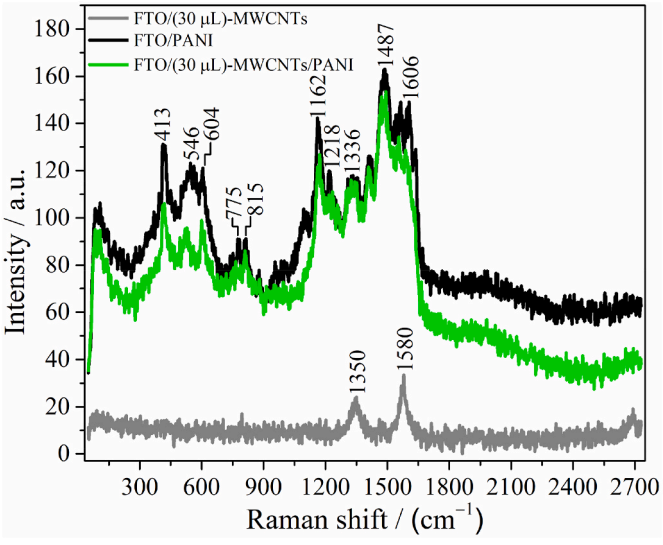

Fig. 6. Raman spectra of FTO/(30 μL)-MWCNTs, FTO/PANI and FTO/(30 μL)-MWCNTs/PANI films.

The Raman spectra of the FTO/PANI and FTO/(30 μL)-MWCNTs/PANI films featured the following bands for the polaronic structure: 1606 (C–C stretching) and 604 cm^{-1} (benzenoid ring deformation) [56]. Since only two bands were observed in the Raman spectra for the polaronic structure and supported by the analyses of the absorbance (see Fig. 4a) and ATR-FTIR spectra (Fig. 5), we believe that the polaronic structure is present as a minority phase, whereas the bipolaronic structure is the predominant form of the PANI films in the form of emeraldine hydrochloride.

3.2. PEC evaluation of the films

In addition to the physical characterisation, it was also investigated the PEC performance of the FTO/MWCNTs/PANI films via chronoamperometry measurements of the films polarised at −0.5 V and under chopped UV irradiation. As shown in Fig. 7, all the films displayed a cathodic photocurrent density signal upon illumination, suggesting that these materials may possess p-type conductivity behaviour, which is in agreement with the studies reported in the literature [11,57,58]. The cathodic photocurrent density response of the films is probably assigned to the light-driven HER, meaning that H_2 is generated from the reduction of the hydronium ions (H_3O^+) by the photogenerated electrons in the LUMO level (e^-_{LUMO}) of PANI (Equation (1)). Since excitons are probably the dominant photogenerated quasiparticle type in PANI [59], the e^-_{LUMO} as well as the holes in the HOMO level (h^+_{HOMO}) may have been originated from the dissociation of photogenerated excitons within the PANI films under the influence of the applied potential. It is also important to mention that our hypothesis about the occurrence of the HER is chiefly grounded upon the thermodynamically favourable condition of the potential of the LUMO of PANI (it ranges from −1 to −2 V vs. standard hydrogen electrode (SHE)) being more negative than the potential of HER (0 V vs. SHE) [11].

$$2H_3O^+_{(aq)} + 2e^-_{LUMO} \xrightarrow{2h\nu} H_{2(g)} + 2H_2O_{(l)}, \quad \text{Eq. 1}$$

where $h\nu$ is the photon energy.

Still concerning Fig. 7, under illumination, the chronoamperometric profile of the films features photocurrent density spikes, which are assigned to the carriers' recombination process. Interestingly, the exponential spike decay of the FTO/(10 μL)-MWCNTs/PANI and FTO/(30 μL)-MWCNTs/PANI films seem to be higher compared to that of the FTO/(50 μL)-MWCNTs/PANI film. We believe that these differences in exponential spike decays are probably linked to the different amounts of

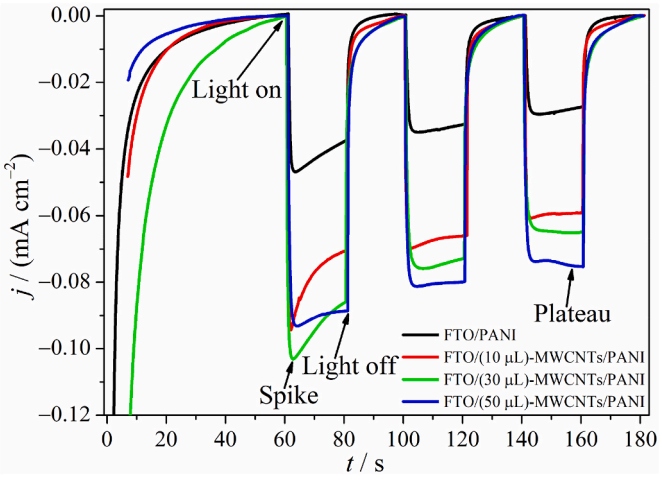

Fig. 7. Chronoamperometry curves at −0.5 V vs. Ag/AgCl/$Cl^-_{(sat.\ KCl)}$ and under chopped UV illumination (irradiance of ca. 100 mW cm^{-2}) of PANI films grown on bare and coated FTO substrates with different amounts of MWCNTs. The electrolyte was a N_2-saturated solution of 0.5 mol L^{-1} Na_2SO_4 at pH 2.0.

traps/defects present in the PANI. Regarding the photocurrent density values at −0.5 V (it corresponds to −0.18 V vs. reversible hydrogen electrode (RHE)) obtained from the plateau region of the last light on/light off cycle, the PANI films grown on bare FTO substrates delivered a photocurrent density value of ca. −0.027 mA cm^{-2}. The PANI films deposited on FTO substrates coated with 10, 30, and 50 μL of MWCNTs displayed photocurrent density values of ca. −0.059, −0.065, and −0.076 mA cm^{-2}, respectively. The highest enlargements of photocurrent density were achieved for the FTO/(30 μL)-MWCNTs/PANI (2.4 fold) and FTO/(50 μL)-MWCNTs/PANI (2.8 fold) films compared to that of the FTO/PANI film.

Besides the PEC activity, we have also evaluated the PEC stability of the FTO/PANI and FTO/MWCNTs/PANI films using chronoamperometry measurements at −0.5 V and under continuous UV illumination, as displayed in Fig. 8. Regarding the FTO/PANI film, it was not noted obvious cathodic photocurrent density decay in the plateau region (i.e., after spike formation), which suggests good stability for this film. The chronoamperometry curve of the FTO/PANI film also featured approximately 22% cathodic photocurrent density increase (from 2000 s until the illumination was ceased). Although more studies are required, we believe that FTO/PANI film could have undergone photo-induced superficial modifications, and this may have favoured the percentage increase of cathodic photocurrent density. Concerning the PEC stability of the FTO/MWCNTs/PANI film, it was observed, in the plateau region, a considerable cathodic photocurrent density decay of more than 45% for the FTO/(10 μL)-MWCNTs/PANI film, whose photocurrent density reached a value, at the end of the stability test, comparable to the one obtained for the FTO/PANI film. Conversely, a better PEC stability condition was achieved for the FTO/(30 μL)-MWCNTs/PANI and the FTO/(50 μL)-MWCNTs/PANI films, as observed by their relatively low cathodic photocurrent density decay of up to 7% within 3720 s of stability test. Based on these PEC analyses, we have found that growing PANI films on FTO substrates coated with 30 μL of MWCNTs is the minimum amount required to achieve a good PEC performance (i.e., activity and stability) for the light-driven HER.

Additional PEC analyses based on EIS experiments were carried out aiming to have a further understanding of the PEC performance improvement achieved for the FTO/(30 μL)-MWCNTs/PANI film, i.e., the optimum condition. For comparison purposes, EIS experiments were also performed for the FTO/PANI film. The impedance spectra were obtained for these films polarised at −0.5 V, and under UV illumination, as depicted in Fig. 9. The complex-plane impedance diagram of both

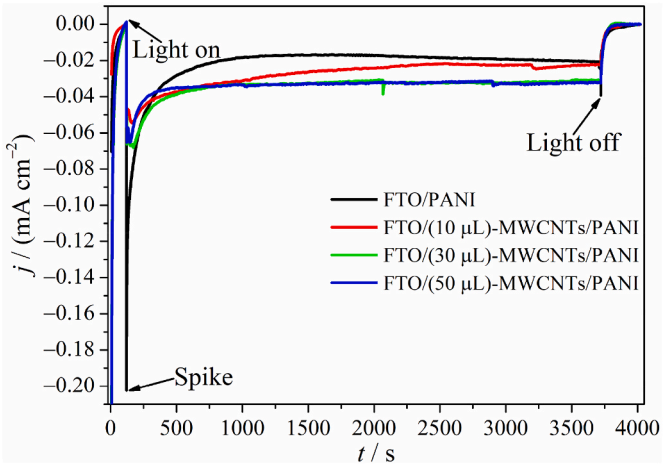

Fig. 8. Chronoamperometry curves at −0.5 V vs. $Ag/AgCl/Cl^-_{(sat.\ KCl)}$ and under continuous UV illumination (irradiance of ca. 100 mW cm^{-2}) for the PEC stability tests of PANI films grown on bare and coated FTO substrates with different amounts of MWCNTs. The electrolyte was a N_2-saturated solution of 0.5 mol L^{-1} Na_2SO_4 at pH 2.0.

films (Fig. 9a) featured one semicircle formation tendency, suggesting the occurrence of at least one charge transfer process. Supporting this hypothesis, the Bode diagram (see Fig. 9b) of both films also displayed only one peak of phase angle (φ), which might be assigned to at least one charge transfer process and that can be designated to at least one time constant (τ) defined as $\tau = RC$, where R is the resistance and C and the capacitance density of the charge transfer process. Since there was one semicircle and one φ peak, we have fitted the EIS spectra into an equivalent circuit comprised of one RC component connected in series with a solution resistance (R_s), as shown in the inset of Fig. 9a. To account for the non-ideal capacitor behaviour of the double-layer, we have employed a constant phase element (CPE) instead of an ideal capacitor and the real value of the C obtained from the CPE was determined according to Equation (2) [60].

$$C = \frac{(QR)^{1/\alpha_f}}{R}, \qquad \text{Eq.2}$$

where Q is the pseudocapacitance density, also known as CPE-T, and α_f is the CPE exponent, also known as CPE-P. The α_f varies from 0 to 1, being the unity value associated with the CPE behaving like an ideal capacitor.

The calculated C values and all the fitted parameters obtained for the FTO/PANI and FTO/(30 μL)-MWCNTs/PANI films are listed in Table 1. The percentage fitting error values of each element in the equivalent circuit as well as the chi-squared values are summarised in Table S1.

According to the fitting results from Table 1, the R, or more specifically the R_{ct}, of FTO/(30 μL)-MWCNTs/PANI film featured a 1.85-fold decrease compared to that of the FTO/PANI film. This diminished R_{ct} value suggests that the transfer of the photogenerated e^-_{LUMO} at the polymer|electrolyte interface was facilitated, which could have been the reason for the photoresponse enhancement of the FTO/(30 μL)-MWCNTs/PANI film (see Figs. 7 and 8). It is also noted from Table 1 that the C_d value of the FTO/(30 μL)-MWCNTs/PANI film was 2.74 times higher in comparison with the value obtained for the FTO/PANI film. Since C_d is known to be directly proportional to the electrode surface area [61], the increase in C_d value could have been due to the increased surface area of FTO/(30 μL)-MWCNTs/PANI film compared to that of FTO/PANI film. Moreover, as shown in the SEM micrographs (Figure S2), the surface of FTO/(30 μL)-MWCNTs/PANI film seems to be rougher than that of FTO/PANI film, which supports our hypothesis about the increased surface area of the FTO/(30 μL)-MWCNTs/PANI film. The possible increase of the surface area of the FTO/(30 μL)-MWCNTs/PANI film may have also contributed to improving its photoresponse, as observed in Figs. 7 and 8.

Aspiring to gain more knowledge about the PEC performance of FTO/PANI and FTO/(30 μL)-MWCNTs/PANI films, Bode diagrams (Fig. 9b) and Equation (3) were employed to estimate the electron lifetime (τ_n) [62].

$$\tau_n = \frac{1}{2\pi f_{max}}, \qquad \text{Eq. 3}$$

where f_{max} is the frequency that corresponds to the maximum φ in the Bode diagrams.

Taking the f_{max} values displayed in Fig. 9b and applying them in Equation (3), it was obtained τ_n estimation of 29.7 and 47.5 ms for FTO/PANI and FTO/(30 μL)-MWCNTs/PANI films, respectively. As noted, the FTO/(30 μL)-MWCNTs/PANI presented longer τ_n, meaning that the presence of the MWCNTs hindered the electron-hole recombination process, and that could have led to photoresponse enhancement of the FTO/(30 μL)-MWCNTs/PANI film, as depicted in Figs. 7 and 8. This minimisation of electron-hole recombination process in the FTO/(30 μL)-MWCNTs/PANI film may be linked to the MWCNTs' capability of collecting and transporting holes as reported in the literature [63–65], and such a collection could have resulted in the longer τ_n. Although more studies are required, the transport of holes from PANI to MWCNTs is perhaps due to the work function of MWCNTs (−4.95 eV vs. vacuum

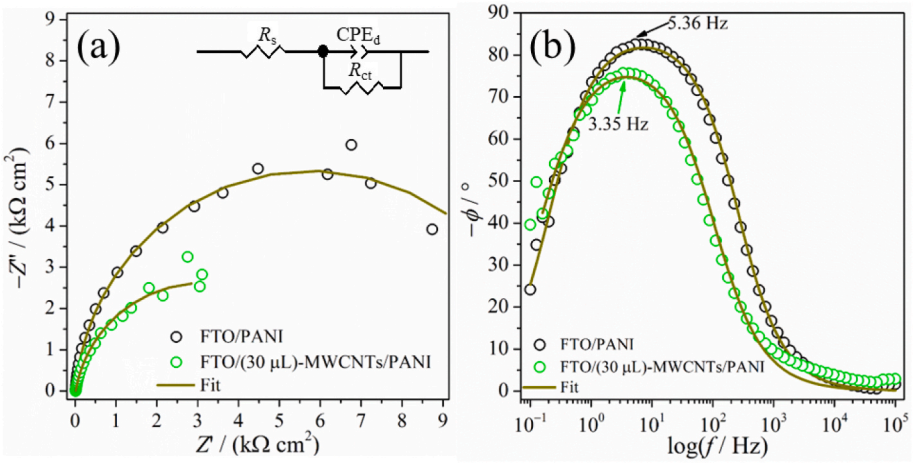

Fig. 9. (a) Complex-plane impedance diagrams and their corresponding (b) Bode diagrams of FTO/PANI and FTO/(30 μL)-MWCNTs/PANI films polarised at −0.5 V vs. Ag/AgCl/$Cl^-_{(sat.\ KCl)}$ and under UV illumination. The electrolyte was a N_2-saturated solution of 0.5 mol L^{-1} Na_2SO_4 at pH 2.0.

Table 1
Resistances and capacitance densities values obtained from the EIS spectra fitting of FTO/PANI and FTO/(30 μL)-MWCNTs/PANI films.

Sample	R_s Ω cm^2	R_{ct}[a] kΩ cm^2	Q_d[b] (α_f) Ω^{-1} cm^{-2} s$^{\alpha f}$	C_d[c] μF cm^{-2}
FTO/PANI	13.3	11.5	6.67×10^{-5} (0.95)	65.8
FTO/(30 μL)-MWCNTs/PANI	16.9	6.20	1.78×10^{-4} (0.90)	180.0

[a] R_{ct} is the charge transfer resistance.
[b] Q_d is the double-layer pseudocapacitance density.
[c] C_d is the real double-layer capacitance density.

[66]) being less negative than the HOMO energy level of PANI (ca. −5.13 eV vs. vacuum [67]). It is also interesting to mention that studies have been reported that the MWCNTs|polymer interface may act as sites for the dissociation of the excitons into free charge carriers (i.e., electrons and holes) [68–71], which may be followed by, eventually, the collection of holes by the MWCNTs and the transfer of electrons at the polymer|electrolyte interface to drive, e.g., the HER. Based on this, the probable dissociation of PANI's photogenerated excitons at the MWCNTs|PANI interface may have been an additional contribution of the MWCNTs for the PEC HER improvement of the FTO/MWCNTs/PANI films, as shown in Fig. 7. The presence of the (30 μL)-MWCNTs layer underneath PANI films also contributed to improving light absorption of this system (see the absorbance increase in the UV–vis–NIR spectra of Fig. 4a), which was assigned to the multiple reflections inside the porous structures (Fig. 3) of the FTO/(30 μL)-MWCNTs/PANI film, as discussed previously. The absorbance increase of this film stands advantageously since a greater number of excitons may be photogenerated and its electrons (i.e., originated from the dissociation of the excitons) could be used to ultimately drive the HER.

On the strength of what has been presented, we believe that the presence of the MWCNTs layer beneath PANI films improved the photoelectroactivity of the PANI films for the HER due to the following combined effects: (i) enhancement of light absorption due to the light-trapping effect; (ii) possible improvement of excitons dissociation at the MWCNTs|PANI interface; (iii) minimisation of the recombination process due to the holes collection by the MWCNTs layer; and (iv) facilitation of electrons transfer at the PANI|electrolyte interface due to the diminished R_{ct} of the FTO/MWCNTs/PANI films. To better illustrate the combined effects of the aforementioned factors on the PEC improvement of the FTO/MWCNTs/PANI films for the HER, all these factors are summarised in Fig. 10.

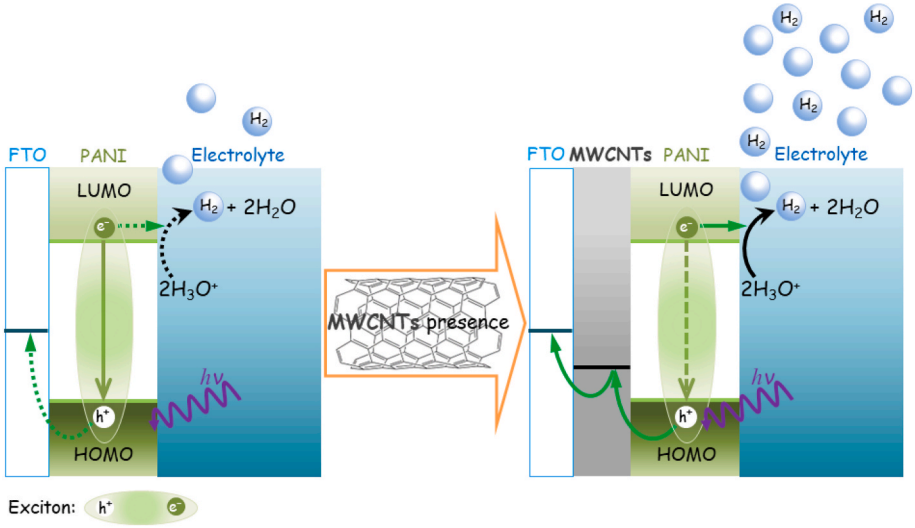

Fig. 10. Schematic representation of the combined contribution of different factors towards the improvement of PEC HER on the FTO/MWCNTs/PANI films.

4. Conclusions

To sum up, we have successfully obtained PANI films via in situ chemical oxidative polymerisation onto bare and coated FTO substrates with different amounts of MWCNTs. Both FTO/PANI and FTO/MWCNTs/PANI films featured PANI in the form of emeraldine hydrochloride and bipolaronic form is probably the major structure, as experimentally evidenced by joint analyses of different characterisation techniques. Regarding the PEC performance of the films, it was found that FTO/MWCNTs/PANI films featuring MWCNTs layer deposited with 30 μL was the optimum condition that provided a 2.4-fold increase of the cathodic photocurrent density response for the HER compared to that of FTO/PANI film. It was also achieved good PEC stability for the optimised films, i.e., FTO/(30 μL)-MWCNTs/PANI, as observed by the relatively low cathodic photocurrent density decay of up to 7% during 3720 s of stability test. The improved PEC performance for the FTO/(30 μL)-MWCNTs/PANI films was assigned to the combined contribution of different factors. The first factor was the improvement of light absorption via the light-trapping capability of the porous structure of the FTO/(30 μL)-MWCNTs/PANI films, as observed by the absorbance spectra and SEM micrographs. Another positive factor is the possible role of the MWCNTs layer in the dissociation of photogenerated excitons from PANI at the MWCNTs|PANI interface. The presence of the MWCNTs layer may have also contributed to the suppression of the electron-hole recombination (as evidenced by the longer τ_n) via the collection and transportation of the holes generated in the HOMO level of PANI. Standing also as another contributing factor is the facilitation of the electrons transfer at the PANI|electrolyte interface for the light-driven HER, as observed by the diminished R_{ct} value of the FTO/(30 μL)-MWCNTs/PANI films. Considering these results, the present study demonstrates improvement of PEC HER on a carbon-based photocathode and to achieve PEC activity and stability comparable to the inorganic photocathodes as well as for technological applications, future studies should focus on additional modifications to further enhance excitons dissociation and interfacial transfer of charge carriers as well.

CRediT authorship contribution statement

Alessandra A. Correa: Writing – review & editing, Writing – original draft, Methodology, Investigation, Funding acquisition, Formal analysis, Data curation, Conceptualization. **Moisés A. de Araújo:** Writing – review & editing, Writing – original draft, Methodology, Investigation, Funding acquisition, Formal analysis, Data curation, Conceptualization. **Lucia H. Mascaro:** Writing – review & editing, Writing – original draft, Visualization, Supervision, Formal analysis. **Luiz H.C. Mattoso:** Writing – review & editing, Writing – original draft, Visualization, Supervision, Formal analysis. **José M. Marconcini:** Writing – review & editing, Writing – original draft, Supervision, Data curation, Conceptualization.

Declaration of competing interest

The authors declare that they have no known competing financial interests or personal relationships that could have appeared to influence the work reported in this paper.

Data availability

No data was used for the research described in the article.

Acknowledgements

This study was financed in part by the Coordenação de Aperfeiçoamento de Pessoal de Nível Superior - Brasil (CAPES) - Finance Code 001 (Proc. 88887.362974/2019-00). It was funded by grant #2016/12681-0, #2013/07296-2, #2017/11986-5, and #2018/22214-6, São Paulo Research Foundation (FAPESP). It was also funded by the Conselho Nacional de Pesquisa e Desenvolvimento (CNPq) grant number #152607/2022-6, #311769/2022-5, #406156/2022-0 and #304044/2019-9, Rede AgroNano/Embrapa (21.1403.001.00.00) and SISNANO/CNPq-MCTI (442575-2019-0), and Financiadora de Estudos e Projetos (FINEP) #grant number 01.22.0179.00. The authors also thank Shell and the strategic importance of the support given by ANP (Brazil's National Oil, Natural Gas, and Biofuels Agency) through the R&D levy regulation. We are also very much indebted to Dr Júlio C. Sczancoski from Universidade Federal de São Carlos (UFSCar) who carefully performed the Raman experiments.

Appendix A. Supplementary data

Supplementary data to this article can be found online at https://doi.org/10.1016/j.polymer.2024.126869.

References

[1] S.E. Hosseini, M.A. Wahid, Hydrogen production from renewable and sustainable energy resources: promising green energy carrier for clean development, Renew. Sust. Energ. Rev. 57 (2016) 850–866, https://doi.org/10.1016/j.rser.2015.12.112.
[2] B. Moss, O. Babacan, A. Kafizas, A. Hankin, A review of inorganic photoelectrode developments and reactor scale-up challenges for solar hydrogen production, Adv. Energy Mater. 11 (2021) 2003286, https://doi.org/10.1002/aenm.202003286.
[3] S. Bellani, M.R. Antognazza, F. Bonaccorso, Carbon-based photocathode materials for solar hydrogen production, Adv. Mater. (2018) 1801446–18014479, https://doi.org/10.1002/adma.201801446.
[4] M.A. de Araújo, M.B. Costa, L.H. Mascaro, Improved photoelectrochemical hydrogen gas generation on Sb_2S_3 films modified with an earth-abundant MoS_x Co-catalyst, ACS Appl. Energy Mater. 5 (2022) 1010–1022, https://doi.org/10.1021/acsaem.1c03374.
[5] M.A. de Araújo, L.H. Mascaro, Plasma treatment: a novel approach to improve the photoelectroactivity of Sb_2S_3 thin films to water splitting, Chemelectrochem 7 (2020) 2325–2329, https://doi.org/10.1002/celc.202000496.
[6] M.V. de L. Tinoco, M.B. Costa, L.H. Mascaro, J.F. de Brito, Photoelectrodeposition of Pt nanoparticles on Sb_2Se_3 photocathodes for enhanced water splitting, Electrochim. Acta 382 (2021) 138290, https://doi.org/10.1016/j.electacta.2021.138290.
[7] W. Yang, J. Moon, Rapid advances in antimony triselenide photocathodes for solar hydrogen generation, J. Mater. Chem. A 7 (2019) 20467, https://doi.org/10.1039/c9ta07990d.
[8] C.Y. Toe, S. Zhou, M. Gunawan, X. Lu, Y.H. Ng, R. Amal, Recent advances and the design criteria of metal sulfide photocathodes and photoanodes for photoelectrocatalysis, J. Mater. Chem. A 9 (2021) 20277–20319, https://doi.org/10.1039/D1TA05407D.
[9] M. Thangamuthu, Q.R.P.O. Ohemeng, B. Luo, D. Jing, R. Godin, J. Tang, Polymer photoelectrodes for solar fuel production: progress and challenges, Chem. Rev. 122 (2022) 11778–11829, https://doi.org/10.1021/acs.chemrev.1c00971.
[10] K. Oka, H. Nishide, B. Winther-Jensen, Completely solar-driven photoelectrochemical water splitting using a neat polythiophene film, Cell Rep. Phys. Sci. 2 (2021) 100306, https://doi.org/10.1016/j.xcrp.2020.100306.
[11] O.S. Ekande, M. Kumar, Review on polyaniline as reductive photocatalyst for the construction of the visible light active heterojunction for the generation of reactive oxygen species, J. Environ. Chem. Eng. 9 (2021) 105725, https://doi.org/10.1016/j.jece.2021.105725.
[12] C. Oueiny, S. Berlioz, F.-X. Perrin, Carbon nanotube–polyaniline composites, Prog. Polym. Sci. 39 (2014) 707–748, https://doi.org/10.1016/j.progpolymsci.2013.08.009.
[13] T.M. Clarke, J.R. Durrant, Charge photogeneration in organic solar cells, Chem. Rev. 110 (2010) 6736–6767, https://doi.org/10.1021/cr900271s.
[14] C. Dai, Y. Pan, B. Liu, Conjugated polymer nanomaterials for solar water splitting, Adv. Energy Mater. (2020) 2002474, https://doi.org/10.1002/aenm.202002474.
[15] Y. Gong, J. Wang, Z. Wei, P. Zhang, H. Li, Y. Wang, Combination of carbon nitride and carbon nanotubes: synergistic catalysts for energy conversion, ChemSusChem 7 (2014) 2303–2309, https://doi.org/10.1002/cssc.201402078.
[16] M. Zhong, M. Zhang, X. Li, Carbon nanomaterials and their composites for supercapacitors, Carbon Energy (2022) 950–985, https://doi.org/10.1002/cey2.219.
[17] C. Ming, S. Leng-Leng, Review on the recent progress of carbon counter electrodes for dye-sensitized solar cells, J. Chem. Eng. 304 (2016) 629–645, https://doi.org/10.1016/j.cej.2016.07.001.
[18] A. Suryawanshi, P. Dhanasekaran, D. Mhamane, S. Kelkar, S. Patil, N. Gupta, S. Ogale, Doubling of photocatalytic H_2 evolution from g-C_3N_4 via its nanocomposite formation with multiwall carbon nanotubes: electronic and morphological effects, Int. J. Hydrog. Energy 37 (2012) 9584–9589, https://doi.org/10.1016/j.ijhydene.2012.03.123.
[19] Y. Chen, J. Li, Z. Hong, B. Shen, B. Lin, B. Gao, Origin of the enhanced visible-light photocatalytic activity of CNT modified g-C_3N_4 for H_2 production, Phys. Chem. Chem. Phys. 16 (2014) 8106–8113, https://doi.org/10.1039/C3CP55191A.

[20] G.B. Pour, H. Ashourifar, L.F. Aval, S. Solaymani, CNTs-supercapacitors: a review of electrode nanocomposites based on CNTs, graphene, metals, and polymers, Symmetry 15 (2023) 1179, https://doi.org/10.3390/sym15061179.

[21] H.N. Heme, M.S.N. Alif, S.M.S.M. Rahat, S.B. Shuchi, Recent progress in polyaniline composites for high capacity energy storage: a review, J. Energy Storage 42 (2021) 103018–103042, https://doi.org/10.1016/j.est.2021.103018.

[22] J. Banerjee, K. Dutta, M.A. Kader, S.K. Nayak, An overview on the recent developments in polyaniline-based supercapacitors, Polym. Adv. Technol. 30 (2019) 1902–1921, https://doi.org/10.1002/pat.4624.

[23] C. Zhang, H. Li, Y. Liu, P. Li, S. Liu, C. He, Advancement of polyaniline/carbon nanotubes based thermoelectric composites, Materials 15 (2022) 8644, https://doi.org/10.3390/ma15238644.

[24] A.H. Majeed, L.A. Mohammed, O.G. Hammoodi, S. Sehgal, M.A. Alheety, K. K. Saxena, S.A. Dadoosh, I.K. Mohammed, M.M. Jasim, N.U. Salmaan, A review on polyaniline: synthesis, properties, nanocomposites, and electrochemical applications, Int. J. Polym. Sci. (2022) 1–19, https://doi.org/10.1155/2022/9047554.

[25] A. Krishnan, T.C. Bhagya, S.M.A. Shibli, Facile synthesis of a versatile Ti/Ti-W@PANI nanocomposite for sustainable hydrogen production under solar irradiation, Appl. Surf. Sci. 507 (2020) 145093, https://doi.org/10.1016/j.apsusc.2019.145093.

[26] S. Sk, A. Tiwari, B.M. Abraham, N. Manwar, V. Perupogu, U. Pal, Constructing Cu/BN@PANI ternary heterostructure for efficient photocatalytic hydrogen generation: a combined experimental and DFT studies, Inter. J. Hydrogen Energy 46 (2021) 27394–27408, https://doi.org/10.1016/j.ijhydene.2021.06.033.

[27] R.A. Galvão, G.M.M. Silva, N.C. Ferreira Coêlho, L.A. Santa-Cruz, G. Machado, Hydrogen production by the layer-by-layer assembled films of PAni-TiO_2-AuNPs, Mater. Today Chem. 26 (2022) 101072, https://doi.org/10.1016/j.mtchem.2022.101072.

[28] E. Belarb, V.M. Blas-Ferrando, M. Haro, H. Maghraoui-Meherzi, S. Gimenez, Electropolymerized polyaniline: a promising hole selective contact in organic photoelectrochemical cells, Chem. Eng. Sci. 154 (2016) 143–149, https://doi.org/10.1016/j.ces.2016.06.055.

[29] O.-K. Park, N.H. Kim, G.-H. Yoo, K.Y. Rhee, J.H. Lee, Effects of the surface treatment on the properties of polyaniline coated carbon nanotubes/epoxy composites, Compos. B Eng. 41 (2010) 2–7, https://doi.org/10.1016/j.compositesb.2009.10.002.

[30] A. Singh, C. Sguazzo, C.F.R.A.C. Lima, L.M.N.B.F. Santos, J.M. Reis, P.M.G. P. Moreira, P.J.S. Tavares, Oxidative treatment of multi-walled carbon nanotubes and its effect on the mechanical and electrical properties of green epoxy based nano-composites, Procedia Struct. Integr. 17 (2019) 857–864, https://doi.org/10.1016/j.prostr.2019.08.114.

[31] M.A. de Araújo, F.W.S. Lucas, L.H. Mascaro, Effect of the electrodeposition potential on the photoelectroactivity of the SnS/Sb_2S_3 thin films, J. Solid State Electrochem. 24 (2020) 389–399, https://doi.org/10.1007/s10008-020-04508-2.

[32] A.G. MacDiarmid, A.J. Epstein, Polyanilines: a novel class of conducting polymers, Faraday Discuss 91 (1991) 1–496, https://doi.org/10.1039/DC9898800317.

[33] M. Canales, J. Torras, G. Fabregat, A. Meneguzzi, C. Alemán, Polyaniline emeraldine salt in the amorphous solid state: polaron versus bipolaron, J. Phys. Chem. B 118 (2014) 11552–11562, https://doi.org/10.1021/jp5067583.

[34] J. Stejskal, I. Sapurina, Polyaniline: thin films and colloidal dispersions, Pure Appl. Chem. 77 (2005) 815–826, https://doi.org/10.1351/pac200577050815.

[35] I. Sapurina, A. Riede, J. Stejskal, In-situ polymerized polyaniline films: 3. film formation, Synth. Met. 123 (2001) 503–507, https://doi.org/10.1016/S0379-6779(01)00349-6.

[36] X. Wang, D. Wu, X. Song, W. Du, X. Zhao, D. Zhang, Review on carbon/polyaniline hybrids: design and synthesis for supercapacitor, Molecules 24 (2019) 2263–2281, https://doi.org/10.3390/molecules24122263.

[37] R.C.Y. King, F. Roussel, J.-F. Brun, C. Gors, Carbon nanotube-polyaniline nanohybrids: influence of the carbon nanotube characteristics on the morphological, spectroscopic, electrical and thermoelectric properties, Synth. Met. 162 (2012) 1348–1356, https://doi.org/10.1016/j.synthmet.2012.05.029.

[38] C. Dhivya, S.A.A. Vandarkuzhali, N. Radha, Antimicrobial activities of nanostructured polyanilines doped with aromatic nitro compounds, Arab. J. Chem. 12 (2019) 3785–3798, https://doi.org/10.1016/j.arabjc.2015.12.005.

[39] T.-M. Wu, Y.-W. Lin, C.-S. Liao, Preparation and characterization of polyaniline/multi-walled carbon nanotube composites, Carbon 43 (2005) 734–740, https://doi.org/10.1016/j.carbon.2004.10.043.

[40] D.K. Kim, K.W. Oh, S.H. Kim, Synthesis of polyaniline/multiwall carbon nanotube composite via inverse emulsion polymerization, J. Polym. Sci. B Polym. Phys. 46 (2008) 2255–2266, https://doi.org/10.1002/polb.21557.

[41] N. Bafandeh, M.M. Larijani, A. Shafiekhani, M.R. Hantehzadeh, N. Sheikh, Effects of contents of multiwall carbon nanotubes in polyaniline films on optical and electrical properties of polyaniline, Chin. Phys. Lett. 33 (2016) 117801, https://doi.org/10.1088/0256-307X/33/11/117801.

[42] G. Chakraborty, K. Gupta, D. Rana, A.K. Meikap, Effect of multiwalled carbon nanotubes on electrical conductivity and magnetoconductivity of polyaniline, Adv. Nat. Sci. Nanosci. Nanotechnol. 3 (2012) 035015, https://doi.org/10.1088/2043-6262/3/3/035015.

[43] S. Lal, S.K. Tripathi, N. Sood, S. Khosl, Impact of the concentration of multiwall carbon nanotubes on polyaniline, J. Inf. Disp. 15 (2014) 111–117, https://doi.org/10.1080/15980316.2014.916630.

[44] M. Cochet, W.K. Maser, A.M. Benito, M.A. Callejas, M.T. Martínez, J.-M. Benoit, J. Schreiber, O. Chauvet, Synthesis of a new polyaniline/nanotube composite: "in-situ" polymerisation and charge transfer through site-selective interaction, Chem. Commun. 16 (2001) 1450–1451, https://doi.org/10.1039/b104009j.

[45] S. Chen, D. Huang, G. Zeng, X. Gong, W. Xue, J. Li, Y. Yang, C. Zhou, Z. Li, X. Yan, T. Li, Q. Zhang, Modifying delafossite silver ferrite with polyaniline: visible-light-response Z-scheme heterojunction with charge transfer driven by internal electric field, J. Chem. Eng. 370 (2019) 1087–1100, https://doi.org/10.1016/j.cej.2019.03.282.

[46] A.N. Banerjee, S. Kundoo, P. Saha, K.K. Chattopadhyay, Synthesis and characterization of nano-crystalline fluorine-doped tin oxide thin films by sol-gel method, J. Sol. Gel Sci. Technol. 28 (2003) 105–110, https://doi.org/10.1023/A:1025697322395.

[47] D. Amalric-Popescu, F. Bozon-Verduraz, Infrared studies on SnO_2 and Pd/SnO_2, Catal. Today 70 (2001) 139–154, https://doi.org/10.1016/S0920-5861(01)00414-X.

[48] Y. Furukawa, F. Ueda, Y. Hyodo, I. Harada, T. Nakajima, T. Kawagoe, Vibrational spectra and structure of polyaniline, Macromolecules 21 (1988) 1297–1305, https://doi.org/10.1021/ma00183a020.

[49] H. Zengin, W. Zhou, J. Jin, R. Czerw, D.W. Smith Jr., L. Echegoyen, D.L. Carroll, S. H. Foulger, J. Ballato, Carbon nanotube doped polyaniline, Adv. Mater. 14 (2002) 1480–1483, https://doi.org/10.1002/1521-4095(20021016)14:20<1480::AID-ADMA1480>3.0.CO;2-O.

[50] S. Sharma, S. Singh, N. Khare, Enhanced photosensitization of zinc oxide nanorods using polyaniline for efficient photocatalytic and photoelectrochemical water splitting, Int. J. Hydrog. 41 (2016) 21088–21098, https://doi.org/10.1016/j.ijhydene.2016.08.131.

[51] Y. Yu, B. Che, Z. Si, L. Li, W. Chen, G. Xue, Carbon nanotube/polyaniline core-shell nanowires prepared by in situ inverse microemulsion, Synth. Met. 150 (2005) 271–277, https://doi.org/10.1016/j.synthmet.2005.02.011.

[52] S. Quillard, G. Louarn, S. Lefrant, A.G. Macdiarmid, Vibrational analysis of polyaniline: a comparative study of leucoemeraldine, emeraldine, and pernigraniline bases, Phys. Rev. B 50 (1994) 12496–12508, https://doi.org/10.1103/PhysRevB.50.12496.

[53] S. Sharma, S. Singh, N. Khare, Synthesis of polyaniline/CdS (nanoflowers and nanorods) nanocomposites: a comparative study towards enhanced photocatalytic activity for degradation of organic dye, Colloid Polym. Sci. 294 (2016) 917–926, https://doi.org/10.1007/s00396-016-3844-4.

[54] S.B. Brachetti-Sibaja, D. Palma-Ramírez, A.M. Torres-Huerta, M.A. Domínguez-Crespo, H.J. Dorantes-Rosales, A.E. Rodríguez-Salazar, E. Ramírez-Meneses, CVD conditions for MWCNTs production and their effects on the optical and Eelectrical properties of PPy/MWCNTs, PANI/MWCNTs nanocomposites by in situ electropolymerization, Polymers 13 (2021) 351–380, https://doi.org/10.3390/polym13030351.

[55] M. Cochet, G. Louarn, S. Quillard, J.P. Buisson, S. Lefrant, Theoretical and experimental vibrational study of emeraldine in salt form. Part II, J. Raman Spectrosc. 31 (2000) 1041–1126, https://doi.org/10.1002/1097-4555(200012)31:12<1041::AID-JRS641>3.0.CO;2-R.

[56] J.C. García-Gallegos, Y.I. Vega-Cantú, F.J. Rodríguez-Macías, Fast mechanochemical synthesis of carbon nanotube-polyaniline hybrid materials, J. Mater. Res. 33 (2018) 1486–1495, https://doi.org/10.1557/jmr.2018.56.

[57] C. Belabed, A. Abdi, Z. Benabdelghani, G. Rekhila, A. Etxeberria, M. Trari, Photoelectrochemical properties of doped polyaniline: application to hydrogen photoproduction, Int. J. Hydrog. Energy 38 (2013) 6593–6599, https://doi.org/10.1016/j.ijhydene.2013.03.085.

[58] H.G. Huang, Z.X. Zheng, J. Luo, H.P. Zhang, L.L. Wu, Z.H. Lin, Internal photoemission in polyaniline revealed by photoelectrochemistry, Synth. Met. 123 (2001) 321–325, https://doi.org/10.1016/S0379-6779(01)00298-3.

[59] S. Cha, Y. Hong, J. Yang, I. Maeng, S.J. Oh, K. Jeong, J.-S. Suh, S. Haam, Y.-M. Huh, H. Choi, Ultrafast spin-resolved spectroscopy reveals dominant exciton dynamics in conducting polymer polyaniline, J. Phys. Chem. C 117 (2013) 20371–20375, https://doi.org/10.1021/jp408800j.

[60] W. Yang, T. Moehl, E. Service, S.D. Tilley, Operando analysis of semiconductor junctions in multi-layered photocathodes for solar water splitting by impedance spectroscopy, Adv. Energy Mater. 11 (2021) 2003569–2003579, https://doi.org/10.1002/aenm.202003569.

[61] E. Taer, A. Agustino, R. Farma, R. Taslim, Awitdrus, M. Paiszal, A. Ira, S.D. Yardi, Y.P. Sari, H. Yusra, S. Nurjanah, S.D. Hartati, Z. Aini, R.N. Setiadi, The relationship of surface area to cell capacitance for monolith carbon electrode from biomass materials for supercapacitor aplication, J. Phys. Conf. Ser. 1116 (2018) 1–6, https://doi.org/10.1088/1742-6596/1116/3/032040.

[62] X. Chen, Y. Tang, W. Liu, Efficient dye-sensitized solar cells based on nanoflower-like ZnO photoelectrode, Molecules 22 (2017) 1284–121289, https://doi.org/10.3390/molecules22081284.

[63] S. Paul, B. Rajbongshi, B. Bora, R.G. Nair, S.K. Samdarshi, Organic photovoltaic cells using MWCNTs, New Carbon Mater 32 (2017) 27–34, https://doi.org/10.1016/S1872-5805(17)60104-5.

[64] A. Capasso, L. Salamandra, A. Di Carlo, J.M. Bell, N. Motta, Low-temperature synthesis of carbon nanotubes on indium tin oxide electrodes for organic solar cells, Beilstein J. Nanotechnol. 3 (2012) 524–532, https://doi.org/10.3762/bjnano.3.60.

[65] M.K.A. Mohammed, A.K. Al-Mousoi, S. Singh, A. Kumar, M.K. Hossain, S.Q. Salih, P. Sasikumar, R. Pandey, A.A. Yadav, Z.M. Yaseen, Improving the performance of perovskite solar cells with carbon nanotubes as a hole transport layer, Opt. Mater. 138 (2023) 113702, https://doi.org/10.1016/j.optmat.2023.113702.

[66] M. Shiraishi, M. Ata, Work function of carbon nanotubes, Carbon 39 (2001) 1913–1917, https://doi.org/10.1016/S0008-6223(00)00322-5.

[67] X. Zhang, Z. Lan, S. Cao, J. Wang, Z. Chen, Nanostructured photoelectrochemical solar cells with polyaniline nanobelts acting as hole conductors, Ionics 21 (2015) 1781–1786, https://doi.org/10.1007/s11581-014-1316-8.

[68] N.A. Nismy, K.D.G.I. Jayawardena, A.A.D.T. Adikaari, S.R.P. Silva, Photoluminescence quenching in carbon nanotube-polymer/fullerene films: carbon nanotubes as exciton dissociation centres in organic photovoltaics, Adv. Mater. 23 (2011) 3796–3800, https://doi.org/10.1002/adma.201101549.
[69] B. Pradhan, S.K. Batabyal, A.J. Pal, Functionalized carbon nanotubes in donor/acceptor-type photovoltaic devices, Appl. Phys. Lett. 88 (2006) 93106–93109, https://doi.org/10.1063/1.2179372.
[70] M.-H. Ham, G.L.C. Paulus, C.Y. Lee, C. Song, K. Kalantar-zadeh, W. Choi, J.-H. Ham, M.S. Strano, Evidence for high-efficiency exciton dissociation at polymer/single-walled carbon nanotube interfaces in planar nano-heterojunction photovoltaics, ACS Nano 4 (2010) 6251–6259, https://doi.org/10.1021/nn1019384.
[71] M. Saoudi, B. Zaidi, A.A. Alotaibi, M.G. Althobaiti, E.M. Alosime, R. Ajjel, Polyaniline: doping and functionalization with single walled carbon nanotubes for photovoltaic and photocatalytic application, Polymers 13 (2021) 2595–2610, https://doi.org/10.3390/polym13162595.